Chapter 14
Optical Elements and Keywords, Complements

Abstract This chapter is not a review of the 60+ optical elements of `zgoubi`'s library. They are described in the Users' Guide. One aim here is, regarding some of them, to briefly recall some aspects which may not be found in the Users' Guide and yet addressed, or referred to, in the theoretical reminder sections and in the exercises. This chapter is not a review of the 40+ monitoring and command keywords available in `zgoubi`, either. However it reviews some of the methods used, by keywords such as MATRIX (computation of transport coefficients from sets of rays), FAISCEAU (which produces beam emittance parameters), and others. This chapter in addition recalls the basics of transport and beam matrix methods, in particular it provides the first order transport matrix of several of the optical elements used in the exercises, in view essentially of comparisons with transport coefficients drawn from raytracing, in simulation exercises.

14.1 Introduction

Optical elements are the basic bricks of charged particle beam lines and accelerators. An optical element sequence is aimed at guiding the beam from one location to another while maintaining it confined in the vicinity of a reference optical axis.

`Zgoubi` library offers of collection of about 100 keywords, amongst which about 60 are optical elements, the others being commands (to trigger spin tracking, trigger synchrotron radiation, print out particle coordinates, compute beam parameters, etc.). This library has built over half a century, so it allows simulating most of the optical elements met in real life accelerator facilities. Quite often, elements available provide different ways to model a particular optical component. A bending magnet for instance can be simulated using AIMANT, or BEND, CYCLOTRON, DIPOLE[S][-M], FFAG, FFAG-SPI, MULTIPOL, QUADISEX, or a field map and TOSCA, CARTEMES or POLARMES to handle it. These various keywords have their respective subtleties, though, more on this can be found in the "Optical Elements Versus Keywords" Section of the guide [1, page 227], which tells "Which optical component can be simulated. Which keyword(s) can be used for that purpose". For a complete inventory of optical elements, refer to the "Glossary of Keywords" found at the beginning of PART A [1, page 9] or PART B of the Users' Guide [1, page 227].

Optical elements in `zgoubi` are actually field models, or field modeling methods such as reading and handling field maps. Their role is to provide the numerical integrator with the necessary field vector(s) to push a particle further, and possibly its spin, along a trajectory. The following sections introduce the analytical field models which the simulation exercises resort to.

`Zgoubi`'s coordinate nomenclature, as well as the Cartesian or cylindrical reference frames used in the optical elements and field maps, have been introduced in Sect. 1.2 and Fig. 1.5.

14.2 Drift Space

This is the DRIFT, or ESL (for the French "ESpace Libre") optical element, through which a particle moves on a straight line. From the geometry and notations in Fig. 14.1, with L the length of the drift, coordinate transport satisfies

$$\left|\begin{array}{l} X_f - X_i = L \\ Y_f - Y_i = L\tan T \\ Z_f - Z_i = L\tan P/\cos T \\ \text{path length } d = L/(\cos T\cos P) \end{array}\right. \tag{14.1}$$

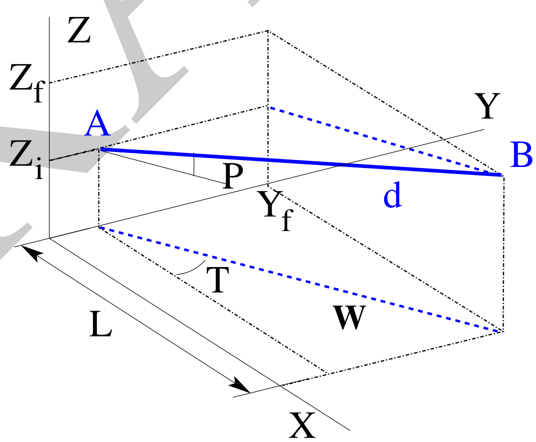

Fig. 14.1 An L-long drift in `zgoubi` (O;X,Y,Z) frame, with origin at the start of the drift. A particle flies from $A(Y_i, Z_i)$ to $B(Y_f, Z_f)$, at an angle P to the (X, Y) plane. Projection W of its straight path in (X, Y) plane is at an angle T to the X axis

Linear approach

Coordinate transport from initial to final position in the linear approximation is written (with z standing indifferently for x or y, subscripts i for initial and f for final coordinates) (Fig. 14.2)

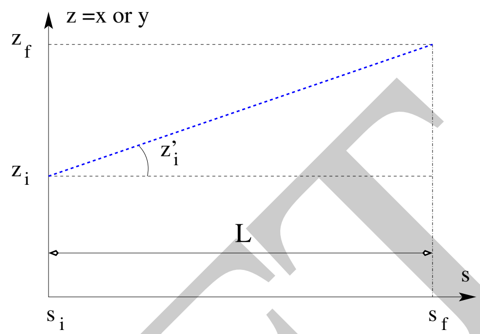

Fig. 14.2 A drift section with length $L = s_f - s_i$, and projection of a straight trajectory in the (s, z) plane, at an angle z' (standing for x' or y') to the s axis

$$\left|\begin{array}{l} z_f = z_i + L\, z_i' \\ z_f' = z_i' \\ \delta l_f - \delta l_i = \beta c \delta t = \dfrac{L}{\gamma^2}\dfrac{\delta p}{p} \\ \delta p_f/p = \delta p_i/p \end{array}\right. \quad \text{or,} \quad T_{\text{drift}} = \begin{pmatrix} 1 & L & 0 & 0 & 0 & 0 \\ 0 & 1 & 0 & 0 & 0 & 0 \\ 0 & 0 & 1 & L & 0 & 0 \\ 0 & 0 & 0 & 1 & 0 & 0 \\ 0 & 0 & 0 & 0 & 1 & \dfrac{L}{\gamma^2} \\ 0 & 0 & 0 & 0 & 0 & 1 \end{pmatrix} \tag{14.2}$$

where βc is the particle velocity, $p = \gamma m \beta c$ its momentum, γ is the Lorentz relativistic factor.

14.3 Guiding

Beam guiding is in general assured using dipole magnets to provide a uniform field, normal to the bend plane. Gradient dipoles combine guiding and focusing in a single magnet, this is the case in cyclotrons, this is also the case in some synchrotrons, for instance the BNL AGS [2], the CERN PS [3]. By principle, FFAG dipoles have pole faces shaped to provide a highly non-linear dipole field, $B \propto r^k$ (Sect. 10). Dipole magnets sometimes include a sextupole component for the compensation of chromatic aberrations [4]. Non-linear optical effects may be introduced by shaping entrance and or exit EFBs, a parabola for instance for x^2 field integral dependence, a cubic curve for x^3 dependence (see Chap. 13).

Low energy beam guiding also uses electrostatic deflectors, shaped to provide a field normal to the trajectory arc, and focusing properties. Plane condensers may be used for beam guiding as well. They are also used at higher energies for some special functions, such as pretzel orbit separation, extraction septa, etc.

Guiding optical elements are dispersive systems: trajectory deflection has a first order dependence on particle momentum.

14.3.1 Dipole Magnet, Curved

This is the DIPOLE element (an evolution of the 1972's AIMANT [1]) or variants: DIPOLES, DIPOLE-M. Lines of constant field are isocentric circle arcs. The magnet reference curve is a particular arc, at a reference radius r_0. The field in the median plane can be written

$$B_Z(r,\theta) = \mathcal{G}(r,\theta)\, B_0 \left(1 + N\,\frac{r-r_0}{r_0} + N'\left(\frac{r-r_0}{r_0}\right)^2 + N''\left(\frac{r-r_0}{r_0}\right)^3 + \ \dots\right) \tag{14.3}$$

$N^{(n)} = d^nN/dY^n$ are the field index and derivatives. $\mathcal{G}(X)$ describes the longitudinal shape of the field, from a plateau value in the body to zero away from the magnet (Fig. 14.3). It can be written under the form

$$\mathcal{G}(X) = G_0\, F(d(X)) \quad \text{with} \quad G_0 = \frac{B_0}{r_0^{n-1}} \tag{14.4}$$

where B_0 is the field at pole tip at r_0, and $F(d)$ a convenient model for the field fall-off, *e.g.* (the Enge model, Sect. 14.3.3),

$$F(d) = \frac{1}{1+\exp[P(d)]}\,, \qquad P(d) = C_0 + C_1\left(\frac{d}{g}\right) + C_2\left(\frac{d}{g}\right)^2 + C_3\left(\frac{d}{g}\right)^3 + \ \dots \tag{14.5}$$

with d (an X-dependent quantity) the distance from (X,Y,Z) location to the magnet EFB, g the characteristic extent of the field fall-off.

Linear approach

The first order transport matrix of a sector dipole with curvature radius ρ, deflection α and index n, in the hard-edge model, writes

$$T_{\text{bend}} = \begin{pmatrix} C_x & S_x & 0 & 0 & 0 & \frac{r_x^2}{\rho}(1-C_x) \\ C'_x & S'_x & 0 & 0 & 0 & \frac{1}{\rho}S_x \\ 0 & 0 & C_y & S_y & 0 & 0 \\ 0 & 0 & C'_y & S'_y & 0 & 0 \\ \frac{1}{\rho}S_x & \frac{r_x^2}{\rho}(1-C_x) & 0 & 0 & 1 & \frac{r_x^3}{\rho^2}(\rho\alpha - S_x) \\ 0 & 0 & 0 & 0 & 0 & 1 \end{pmatrix} \text{ with } \left[\begin{array}{l} C = \cos\frac{\rho\alpha}{r} \\ C' = \frac{dC}{ds} = \frac{1}{\rho}\frac{dC}{d\alpha} = \frac{-S}{r^2} \\ S = r\sin\frac{\rho\alpha}{r} \\ S' = \frac{dS}{ds} = \frac{1}{\rho}\frac{dS}{d\alpha} = C \\ (*)_x :\ r = \rho/\sqrt{1-n} \\ (*)_y :\ r = \rho/\sqrt{n} \end{array}\right. \tag{14.6}$$

or, explicitly,

$$T_{\mathrm{bend}} = \begin{pmatrix} \cos\sqrt{1-n}\,\alpha & \frac{\rho}{\sqrt{1-n}}\sin\sqrt{1-n}\,\alpha & 0 & 0 & 0 & \frac{\rho}{1-n}(1-\cos\sqrt{1-n}\,\alpha) \\ -\frac{\sqrt{1-n}}{\rho}\sin\sqrt{1-n}\,\alpha & \cos\sqrt{1-n}\,\alpha & 0 & 0 & 0 & \frac{1}{\sqrt{1-n}}\sin\sqrt{1-n}\,\alpha \\ 0 & 0 & \cos\sqrt{n}\,\alpha & \frac{\rho}{\sqrt{n}}\sin\sqrt{n}\,\alpha & 0 & 0 \\ 0 & 0 & -\frac{\sqrt{n}}{\rho}\sin\sqrt{n}\,\alpha & \cos\sqrt{n}\,\alpha & 0 & 0 \\ \frac{1}{\sqrt{1-n}}\sin\sqrt{1-n}\,\alpha & \frac{\rho}{1-n}(1-\cos\sqrt{1-n}\,\alpha) & 0 & 0 & 1 & \frac{\rho}{(1-n)^{3/2}}(\sqrt{1-n}\,\alpha - \sin\sqrt{1-n}\,\alpha) \\ 0 & 0 & 0 & 0 & 0 & 1 \end{pmatrix} \tag{14.7}$$

Cancel the index in the previous sector dipole, introduce a wedge angle ε at entrance and exit EFBs. The first order transport matrix, accounting for the entrance and exit EFB wedge focusing (see Sect. 14.4.1), writes

$$T_{\mathrm{bend}} = \begin{pmatrix} \frac{\cos(\alpha-\varepsilon)}{\cos\varepsilon} & \rho\sin\alpha & 0 & 0 & 0 & \rho(1-\cos\alpha) \\ -\frac{\sin(\alpha-2\varepsilon)}{\rho\cos^2\varepsilon} & \frac{\cos(\alpha-\varepsilon)}{\cos\varepsilon} & 0 & 0 & 0 & \frac{\sin(\alpha-\varepsilon)+\sin\varepsilon}{\cos\varepsilon} \\ 0 & 0 & 1-\alpha\tan\varepsilon & \rho\alpha & 0 & 0 \\ 0 & 0 & -\frac{\tan\varepsilon}{\rho}(2-\alpha\tan\varepsilon) & 1-\alpha\tan\varepsilon & 0 & 0 \\ \sin\alpha & 0 & 0 & 0 & 1 & \rho(\alpha-\sin\alpha) \\ 0 & 0 & 0 & 0 & 0 & 1 \end{pmatrix} \tag{14.8}$$

14.3.2 Dipole Magnet, Straight

This is the MULTIPOL element. Lines of constant field are straight lines. An early instance of a straight dipole magnet is the AGS main dipole (Fig. 9.2), which combines steering and focusing, and features in addition a noticeable sextupole component [5]. The multipole components $B_{\mathrm{n}}(X,Y,Z)$ [n=1 (dipole), 2 (quadrupole), 3 (sextupole), ...] in the Cartesian frame of the straight dipole derive, by differentiation, from the scalar potential

$$V_n(X,Y,Z) = (n!)^2 \left(\sum_{\mathrm{q}=0}^{\infty} (-1)^q \, \frac{\mathcal{G}^{(2q)}(X)(Y^2+Z^2)^q}{4^q q!(n+q)!} \right) \left(\sum_{\mathrm{m}=0}^{n} \frac{\sin\left(m\frac{\pi}{2}\right) Y^{n-m} Z^m}{m!(n-m)!} \right) \tag{14.9}$$

where $\mathcal{G}^{(2q)}(X) = d^{2q}\mathcal{G}(X)/dX^{2q}$. In the case of pure dipole field for instance

$$V_1(X,Y,Z) = \mathcal{G}(X)\,Z - \frac{\mathcal{G}''(X)}{8}(Y^2+Z^2) + \frac{\mathcal{G}^{(4)}(X)}{512}(Y^2+Z^2)\,Z \ldots \tag{14.10}$$

and

$$
\begin{aligned}
B_X(X,Y,Z) &= -\frac{\partial V_1}{\partial X} = \quad \mathcal{G}'(X)\,Z - \frac{\mathcal{G}'''(X)}{8}(Y^2+Z^2)\,\ldots \\
B_Y(X,Y,Z) &= -\frac{\partial V_1}{\partial Y} = \qquad -\frac{\mathcal{G}''(X)}{4}\,Y + \frac{\mathcal{G}^{(4)}(X)}{256}\,YZ\,.. \\
B_Z(X,Y,Z) &= -\frac{\partial V_1}{\partial Z} = \mathcal{G}'(X) - \frac{\mathcal{G}''(X)}{4}\,Z + \frac{3\mathcal{G}^{(4)}(X)}{512}Z^2\,\ldots
\end{aligned}
\tag{14.11}
$$

$\mathcal{G}(r,\theta)$ is a longitudinal form factor to account for the field fall-offs at the ends of the magnet, modeled using Eq. 14.5, with distance d to the EFB in the latter, a function of r and θ.

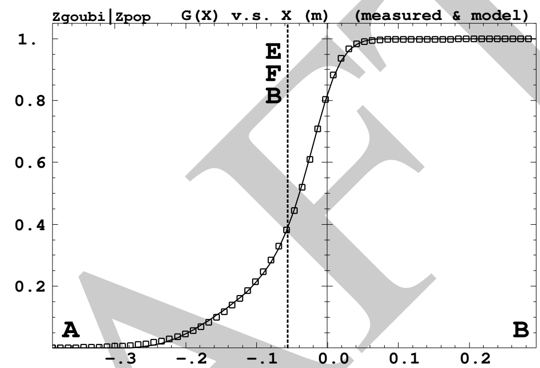

Fig. 14.3 Longitudinal field form factor (Eq. 14.4 - normalized to one) in BNL AGS main bend, taken along the magnet reference axis. Solid line: from Eq. 14.4 with g and C_i values from Eq. 14.14. Squares : measured field data. $X = 0$ is the origin in the field map frame, the vertical dashed line at $X_{\mathrm{EFB}} = -5.62$ cm is the location of the EFB.

14.3.3 Fringe Field, Modeling, Overlapping

A fringe field model is described here, which is resorted to in several optical elements of `zgoubi`'s library.

Field shape at the EFBs of magnetic or electrostatic devices can be simulated using a hard-edge model (the field is assumed to change following a Heaviside step). When using stepwise ray-tracing techniques however, a smooth change of the field can easily be accounted for. An efficient model is Enge's field form factor [6].

$$
F(d) = \frac{1}{1+\exp P(d)} \tag{14.12}
$$

$$
P(d) = C_0 + C_1\left(\frac{d}{\lambda}\right) + C_2\left(\frac{d}{\lambda}\right)^2 + C_3\left(\frac{d}{\lambda}\right)^3 + C_4\left(\frac{d}{\lambda}\right)^4 + C_5\left(\frac{d}{\lambda}\right)^5
$$

where d is the distance to the field boundary and λ is the extent of the fall-off, normally commensurate with gap aperture in a dipole, the radius at pole tip in a quadrupole, etc.

As an illustration, Fig. 14.3 shows $F(d)$ as matched to the measured end fields of BNL AGS main magnet (Fig. 14.3) [7, 8], using

$$\begin{gathered}\lambda = \text{gap aperture} \approx 10\,\text{cm} \quad \text{and} \\ C_0 = 0.45473,\ C_1 = 2.4406,\ C_2 = -1.5088,\ C_3 = 0.7335,\ C_4 = C_5 = 0\end{gathered} \tag{14.13}$$

These C_i coefficient values result from an interpolation to measured field data, which are also represented in the figure. The location of the EFB results from the following constraint, which is part of the matching: the field integral on the down side of the fall-off (the region from A to X=0 in Fig. 14.3) is equal to the complement to 1 of the field integral on the rising side of the fall-off (X=0 to B region in the figure), which writes

$$\int_{\mathrm{X_A}}^{\mathrm{X_{EFB}}} F(X)\,dX = \int_{\mathrm{X_{EFB}}}^{X_B} dX - \int_{\mathrm{X_{EFB}}}^{B} F(X)\,dX \quad \Rightarrow \quad X_{\mathrm{EFB}} = X_B - \int_A^B F(X)\,dX \tag{14.14}$$

A convenient property of this model is that changing the slope of the fall-off (*i.e.*, changing λ) will not affect the location of the EFB.

Inward fringe field extents may overlap when simulating an optical element (Fig. 14.4). A way to ensure continuity of the resulting field form factor in such case is to use

$$F = F_E + F_S - 1 \qquad \text{or} \qquad F = F_E * F_S \tag{14.15}$$

where F_E (F_S) is the entrance (exit) form factor and follows Eq. 14.12. Both expressions can be extended to more than two EFBs (for instance 4, to account for the 4 faces of a dipole magnet: entrance and exit faces, inner and outer radial boundaries). Note that in that case of overlapping field extents, the field integral is affected, lowering with more pronounced overlapping, it is therefore necessary to change the field value (B_0 in Eq. 14.4 for instance) to recover the proper integrated strength.

Overlapping Fringe Fields

`Zgoubi` allows a superposition technique to simulate the field in a series of neighboring magnets. The method consists in computing the mid-plane field at any location (R, θ) by adding individual contributions, namely [9]

$$\begin{gathered}B_Z(r,\theta) = \sum_{\mathrm{i=1,N}} B_{\mathrm{Z,i}}(r,\theta) = \sum_{\mathrm{i=1,N}} B_{\mathrm{Z,0,i}}\, \mathcal{F}_i(r,\theta)\, \mathcal{R}_i(r) \\ \frac{\partial^{k+l}\mathbf{B}_Z(r,\theta)}{\partial\theta^k \partial r^l} = \sum_{\mathrm{i=1,N}} \frac{\partial^{k+l}\mathbf{B}_{\mathrm{Z,i}}(r,\theta)}{\partial\theta^k \partial r^l}\end{gathered} \tag{14.16}$$

with $\mathcal{F}_i(r,\theta)$ and $\mathcal{R}_i(r)$ in each individual dipole in the series (Eqs. 10.7, 10.15). Note that, in doing so it is not meant that field superposition would apply in reality (FFAG magnets are closely spaced, cross-talk may occurs), however it appears to allow closely reproducing magnet computation code outcomes.

Short Optical Elements

In some cases, an optical element in which fringe fields are taken into account (of any kind: dipole, multipole, electrostatic, etc.) may be given small enough a length, L, that it finds itself in the configuration schemed in Fig. 14.4: the entrance and/or the exit EFB field fall-off extends inward enough that it overlaps with the other EFB's fall-off. In zgoubi notations, this happens if $L < X_E + X_S$. As a reminder [1]: in the presence of fringe fields, X_E (resp. X_S) is the stepwise integration extent added upstream (resp. added downstream) of the actual extent L of the optical element.

In such case, `zgoubi` computes field and derivatives along the element using a field form factor $F = F_E \times F_S$. F_E (respectively F_S) is the value of the Enge model coefficient (Eq. 14.12) at distance d_E (resp. d_S) from the entrance (resp. exit) EFB.

This may have the immediate effect, apparent in Fig. 14.4, that the integrated field is not the expected value $B \times L$ from the input data L and B, and may require adjusting (increasing) B so to recover the required BL.

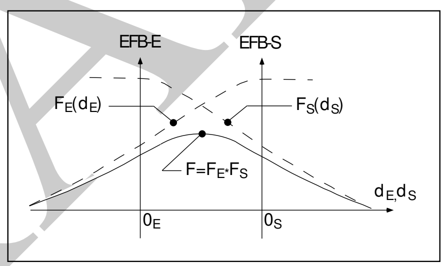

Fig. 14.4 A sketch of overlapping entrance field form factor $F_E(d_E)$ (at the entrance "EFB-E") and exit $F_S(d_S)$ (at the exit "EFB-S"), and resulting form factor $F = F_E \times F_S$ accounted for in modeling the field within the optical element

14.3.4 Toroidal Condenser

This is the ELCYLDEF element in `zgoubi`. With proper parameters, it can be used as a spherical, a toroidal or a cylindrical deflector.

Motion along the optical axis, an arc of a circle of radius r normal to electric field **E**, satisfies

$$Er = v\frac{p}{q} = v(B\rho)$$

with $p = mv$ the particle momentum, q its charge and $(B\rho) = p/q$ the particle rigidity.

The first order transport matrix of an electrostatic bend writes

$$T_{\text{condenser}} = \begin{pmatrix} C_x & S_x & 0 & 0 & 0 & \frac{2-\beta^2}{p_x^2} r_0(1-C_x) \\ C'_x & S'_x & 0 & 0 & 0 & \frac{2-\beta^2}{r_0} S_x \\ 0 & 0 & C_y & S_y & 0 & 0 \\ 0 & 0 & C'_y & S'_y & 0 & 0 \\ -\frac{2-\beta^2}{r_0} S_x & -\frac{2-\beta^2}{p_x^2} r_0(1-C_x) & 0 & 0 & 1 & r_0\alpha\left[\frac{1}{\gamma^2} - \left(\frac{2-\beta^2}{p_x^2}\right)^2 (1-\frac{S_x}{r_0\alpha})\right] \\ 0 & 0 & 0 & 0 & 0 & 1 \end{pmatrix} \tag{14.17}$$

$$\text{with} \begin{cases} \alpha = \text{deflection angle} \\ C = \cos p\alpha \\ C' = \frac{dC}{ds} = -\frac{p^2}{r^2} S \\ S = \frac{r}{p} \sin p\alpha \\ S' = \frac{dS}{ds} = C \\ (*)_x : \ p = p_x = \sqrt{2-\beta^2 - r_0/R_0} \\ (*)_y : \ p = p_y = \sqrt{r_0/R_0} \end{cases}$$

14.4 Focusing

Particle beams are maintained confined along a reference propagation axis by means of focusing techniques and devices. Methods available in `zgoubi` to simulate those are addressed here.

14.4.1 Wedge Focusing

Wedge focusing is sketched in Fig. 14.5. A wedge angle ε causes a particle at local excursion x to experience a change $\int B_y\, ds = xB_y \tan\varepsilon$ of the field integral compared the field integral through the sector magnet, thus in the linear approximation a change in trajectory angle

$$\Delta x' = \frac{1}{B\rho}\int B_y\, ds = x\frac{\tan\varepsilon}{\rho_0} \tag{14.18}$$

with $B\rho$ the particle rigidity and ρ_0 its trajectory curvature radius in the field B_0 of the dipole. Vertical focusing results from the non-zero off-mid plane radial field component B_x in the fringe field region (Fig. 14.7): from (Maxwell's equations) $\frac{\partial}{\partial y}\int B_x\, ds = \frac{\partial}{\partial x}\int B_y\, ds$ and Eq. 14.18 the change in trajectory angle comes out to be

$$\Delta y' = \frac{1}{B\rho}\int B_x\, ds = -y\frac{\tan\varepsilon}{\rho_0} \tag{14.19}$$

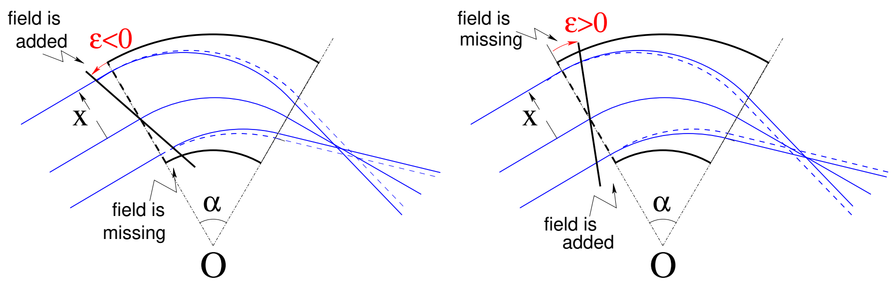

Fig. 14.5 Left: a focusing wedge ($\varepsilon < 0$ by convention); opening the sector increases the horizontal focusing. Right: a defocusing wedge ($\varepsilon > 0$); closing the sector decreases the horizontal focusing. The effect is the opposite in the vertical plane, opening/closing the sector decreases/increases the vertical focusing.

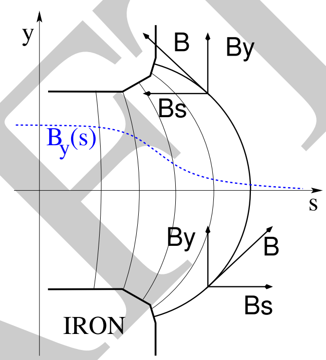

Fig. 14.6 Field components in the $B_y(s)$ fringe field region at a dipole EFB

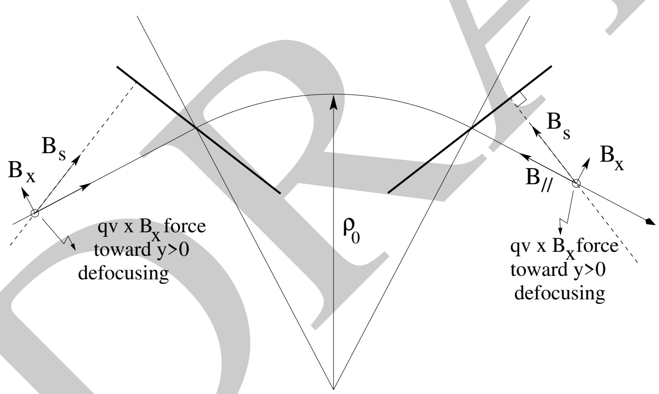

Fig. 14.7 Field components in the fringe field region at the ends of a dipole ($y > 0$, here, referring to Fig. 14.6). $B_{//}$ is parallel to the particle velocity. This configuration is vertically defocusing: a charged particle traveling off mid-plane is pulled away from the the latter under the effect of $\mathbf{v} \times \mathbf{B}_x$ force component. Inspection of the $y < 0$ region gives the same result: the charge is pulled away from the median plane

A first order correction ψ to the vertical kick accounts for the fringe field extent (it is a second order effect for the horizontal kick):

$$\Delta y' = -y\frac{\tan(\varepsilon - \psi)}{\rho_0} \tag{14.20}$$

with

$$\psi = I_1 \frac{\lambda}{\rho_0}\frac{1+\sin^2\varepsilon}{\cos\varepsilon} \quad \text{with} \quad I_1 = \int_{\text{edge}} \frac{B(s)\,(B_0 - B(s))}{\lambda\, B_0^2}\, ds \tag{14.21}$$

λ is the fringe field extent (Sect. 14.3.3), I_1 quantifies the flutter (see Sect. 4.2.1); a longer/shorter field fall-off (smaller/greater flutter) decreases/increases the vertical focusing.

Linear approach

A wedge focusing first order transport matrix writes

$$T_{\text{wedge}} = \begin{pmatrix} 1 & 0 & 0 & 0 & 0 & 0 \\ \frac{\tan\varepsilon}{\rho} & 1 & 0 & 0 & 0 & 0 \\ 0 & 0 & 1 & 0 & 0 & 0 \\ 0 & 0 & -\frac{\tan\varepsilon}{\rho} & 1 & 0 & 0 \\ 0 & 0 & 0 & 0 & 1 & 0 \\ 0 & 0 & 0 & 0 & 0 & 1 \end{pmatrix} \tag{14.22}$$

Substitute $\varepsilon - \psi$ to ε in the R_{43} coefficient, when accounting for fringe field extent λ.

14.4.2 Quadrupole

Most of the time in beam lines and cyclic accelerators, guiding and focusing are separate functions, focusing is assured by quadrupoles, magnetic most frequently, possibly electrostatic at low energy. Quadrupoles are the optical lenses of charged particle beams, they ensure confinement of the beam in the vicinity of the optical axis.

The field in quadrupole lenses results from hyperbolic equipotentials, $V = axy$. Pole profiles in quadrupole lenses follow these equipotentials, in a $2\pi/4$-symmetrical arrangement for technological simplicity.

14.4.2.1 Magnetic Quadrupole

Magnetic quadrupoles are the optical lenses of high energy beams.

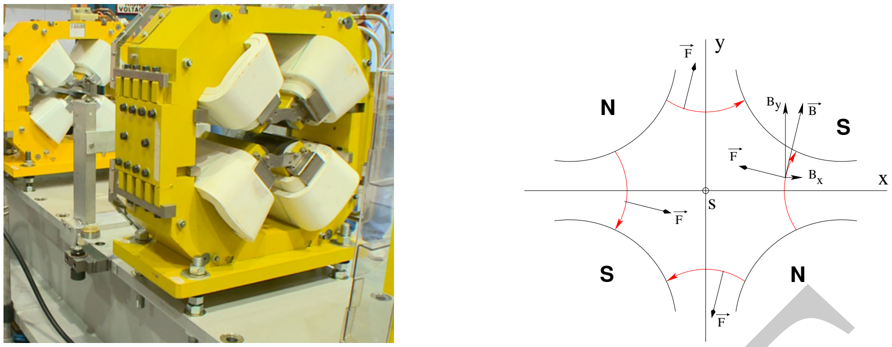

Fig. 14.8 Left: a quadrupole magnet [11]. Right: field lines and forces (assuming positive charges moving out of the page) over the cross section of an horizontally focusing / vertically defocusing quadrupole

The theoretical field in a quadrupole can be derived from Eq. 14.9 for the scalar potential, with $n = 2$ which yields

$$V_2(X,Y,Z) = \mathcal{G}(X)YZ - \frac{\mathcal{G}''(X)}{12}(Y^2+Z^2)YZ + \frac{\mathcal{G}^{(4)}(X)}{384}(Y^2+Z^2)^2YZ - \dots \quad (14.23)$$

and

$$B_X(X,Y,Z) = -\frac{\partial V_2}{\partial X} = \mathcal{G}'(X)YZ - \frac{\mathcal{G}'''(X)}{12}(Y^2+Z^2)YZ + \dots \quad (14.24)$$

$$B_Y(X,Y,Z) = -\frac{\partial V_2}{\partial Y} = \mathcal{G}(X)Z - \frac{\mathcal{G}''(X)}{12}(3Y^2+Z^2)Z + \dots \quad (14.25)$$

$$B_Z(X,Y,Z) = -\frac{\partial V_2}{\partial Z} = \mathcal{G}(X)Y - \frac{\mathcal{G}''(X)}{12}(Y^2+3Z^2)Y + \dots \quad (14.26)$$

$\mathcal{G}(X)$ is given by Eq. 14.4 whereas

$$G_0 = \frac{B_0}{r_0} \quad \text{and} \quad K = G_0/B\rho \quad (14.27)$$

define respectively the quadrupole gradient and strength, the latter relative to the rigidity $B\rho$. The quadrupole is horizontally focusing and vertically defocusing if $K > 0$, and the reverse if $K < 0$, this is illustrated in Fig. 14.9 which shows a doublet of quadrupoles with focusing strengths of opposite signs.

Linear approach

The first order transport matrix of a quadrupole with length L, gradient G and strength $K = G/B\rho$ writes

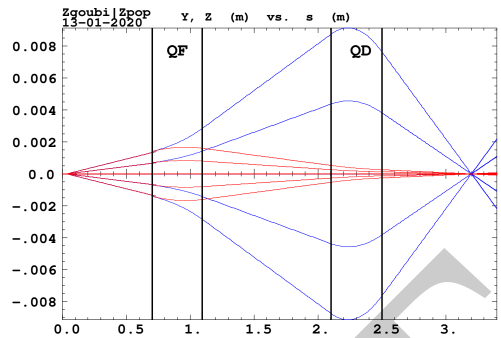

Fig. 14.9 Horizontal and vertical projections of particle trajectories across a stigmatic quadrupole doublet. The first quadrupole (QF) is horizontally focusing ($K > 0$; thus vertically defocusing), the second one (QD) has the reverse sign ($K < 0$)

$$T_{\mathrm{quad}} = \begin{pmatrix} C_x & S_x & 0 & 0 & 0 & 0 \\ C'_x & S'_x & 0 & 0 & 0 & 0 \\ 0 & 0 & C_y & S_y & 0 & 0 \\ 0 & 0 & C'_y & S'_y & 0 & 0 \\ 0 & 0 & 0 & 0 & 1 & \dfrac{L}{\gamma^2} \\ 0 & 0 & 0 & 0 & 0 & 1 \end{pmatrix} \text{ with } \left[\begin{array}{l} C_x = \cos L\sqrt{K};\, C'_x = \frac{dC_x}{dL} = -KS_x \\ S_x = \frac{1}{\sqrt{K}} \sin L\sqrt{K};\, S'_x = \frac{dS_x}{dL} = C_x \\ C_y = \cosh L\sqrt{K};\, C'_y = \frac{dC_y}{dL} = KS_y \\ S_y = \frac{1}{\sqrt{K}} \sinh L\sqrt{K};\, S'_y = \frac{dS_y}{dL} = C_y \end{array} \right. \tag{14.28}$$

$K > 0$ for a focusing quadrupole (by convention, in the (x, x') plane, thus defocusing in the (y, y') plane). Permute the horizontal and vertical 2×2 sub-matrices in the case of a *defocusing* quadrupole.

14.4.2.2 Electrostatic Quadrupole

The hypotheses are those of Sect. 2.2.2: paraxial motion, field normal to velocity, etc. Take the notations of Eqs. 2.25, 2.26 for the field and potential, electrodes in the horizontal and vertical planes (Fig. 2.14). Electrode potential is $\pm V/2$, pole tip radius a, so that $K = -V/2a^2$ in Eq. 2.26. The equations of motion then write

$$\left[\begin{array}{l} \frac{d^2x}{ds^2} + K_x x = 0 \\ \frac{d^2y}{ds^2} + K_y y = 0 \end{array} \right. \quad \text{with } K_x = -K_y = \frac{-qV}{a^2mv^2} = \pm \frac{V}{a^2} \underbrace{\frac{1}{|E\rho|}}_{\substack{\text{electrical} \\ \text{rigidity}}} \tag{14.29}$$

With that $K = \frac{V}{a^2}\frac{1}{|E\rho|} = \frac{V}{a^2}\frac{1}{v(B\rho)}$ value ($(B\rho) = p/q$ is the particle magnetic rigidity), the transport matrix is the same as for the magnetic quadrupole, Eq. 14.28.

14.4.3 Solenoid

Assume a solenoid magnet with (OX) its longitudinal axis, and revolution symmetry, With $(O; X, r, \phi)$ cylindrical frame, radius r, and angle ϕ the coordinates in the X-normal plane, $B_\phi(X, r, \phi) \equiv 0$. Take solenoid length L, mean coil radius r_0 and an asymptotic field $B_0 = \mu_0 NI/L$ with NI = number of ampere-Turns, $\mu_0 = 4\pi \times 10^{-7}$. The asymptotic field value is defined by

$$\int_{-\infty}^{\infty} B_X(X, r < r_0)\, dX = \mu_0 NI = B_0 L \qquad \text{independent of r} \tag{14.30}$$

There is a variety of methods to compute the field vector $\mathbf{B}(X, r)$. Opting for one in particular may be a matter of compromise between computing speed and field modeling accuracy. A simple model is the on-axis field

$$B_X(X, r = 0) = \frac{B_0}{2}\left[\frac{L/2 - X}{\sqrt{(L/2 - X)^2 + r_0^2}} + \frac{L/2 + X}{\sqrt{(L/2 + X)^2 + r_0^2}}\right] \tag{14.31}$$

with $X = r = 0$ taken at the center of the solenoid. This model assumes that the coil thickness is small compared to its mean radius r_0. The magnetic length comes out to be

$$L_{\text{mag}} \equiv \frac{\int_{-\infty}^{\infty} B_X(X, r < r_0) dX}{B_X(X = r = 0)} = L\sqrt{1 + \frac{4r_0^2}{L^2}} > L \tag{14.32}$$

so satisfying

$$\text{on-axis} \;\; B_X(X = r = 0) = \frac{\mu_0 NI}{L\sqrt{1 + \frac{4r_0^2}{L^2}}} \xrightarrow{r_0 \ll XL} \frac{\mu_0 NI}{L}$$

Maxwell's equations and Taylor expansions provide the off-axis field $\mathbf{B}(X, r) = (B_X(X, r), B_r(X, r))$. One has in particular in the $r_0 \ll XL$ limit,

$$B_X(X, r) = \frac{\mu_0 NI}{L} \quad \text{and} \quad B_r(X, r) = \frac{-r}{2}\frac{dB_X}{dX} \tag{14.33}$$

An other way to compute the field vector $\mathbf{B}(X, r)$ is the elliptic integrals technique developed in [12], which constructs $B_X(X, r)$ and $B_r(X, r)$ from respectively

$$B_X(X, r) = \frac{\mu_0 NI}{4\pi}\frac{ck}{r}\,\mathcal{X}\left[K + \frac{r_0 - r}{2r_0}(\Pi - K)\right] \tag{14.34}$$

$$B_r(X, r) = \mu_0 NI \frac{1}{k}\sqrt{\frac{r_0}{r}}\;\left[2(K - E) - k^2 K\right]$$

wherein K, E and Π are the three complete elliptic integrals, $\mathcal{X}$ is an X- and L-dependent form factor, and

$$k = 2\sqrt{r_0 r}/\sqrt{(r_0+r)^2+\mathcal{X}^2}\ ;\ \ c = 2\sqrt{r_0 r}/(r_0+r)$$

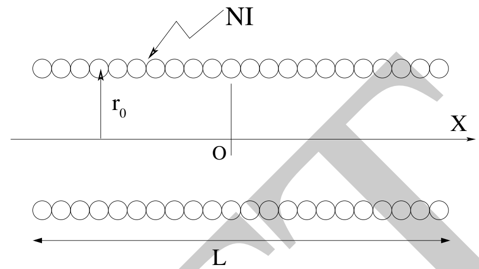

Fig. 14.10 A sketch of a solenoid, and quantities used to define it

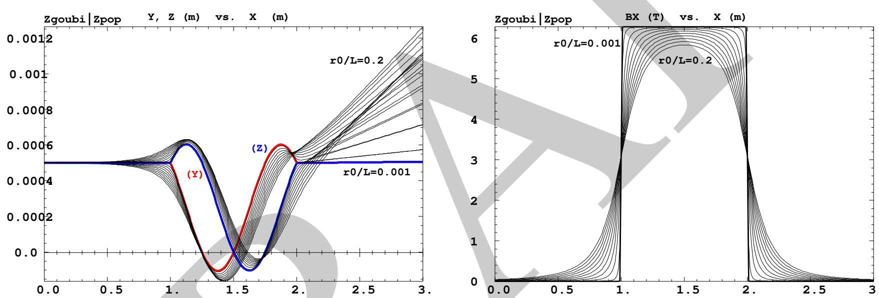

Fig. 14.11 Left: Horizontal (Y) and vertical (Z) projections of a particle trajectory across a $L = 1$ m solenoid, with additional 1 m extents upstream and downstream of the coil. The particle is launched with zero incidence, from transverse position $Y = Z = 0.5$ mm. Sample solenoid radius/length values in the range $0.001 \leq r_0/L \leq 0.2$ show that only for smallest $r_0/L = 0.001$ does the trajectory end with $Y = Z = 0.5$ mm and quasi-zero incidence (the thicker Y(X) and Z(X) curves), whereas greater r_0/L causes final Y(X) and Z(X) to be kicked away. Right: field $B_X(X, r)$ experienced along the trajectory for the various r_0/L values, the steep fall-off case is for $r_0/L = 0.001$.

As an illustration, Fig. 14.11 displays a trajectory across a $L = 1$ m solenoid and its fringe field extents, and the field experienced along that trajectory, in the axial model of Eq. 14.31. In the paraxial approximation, a pitch requires a distance $l = 2\pi/K$, with $K = B_0/B\rho$ the solenoid strength, which is a condition satisfied here if the fringe field extent is short enough (r_0 is small enough).

Linear approach

The equations of motion write, to the first order in the coordinates, in respectively the central region (field B_s) and at the ends (at $s = s_{\mathrm{EFB}}$),

$$\left| \begin{array}{l} x'' - K\,z' = 0 \\ z'' + K\,x' = 0 \end{array} \right. \qquad \text{and} \qquad \left| \begin{array}{l} x'' - \dfrac{K}{2}\,z\,\delta(s - s_{\mathrm{EFB}}) = 0 \\ z'' + \dfrac{K}{2}\,x\,\delta(s - s_{\mathrm{EFB}}) = 0 \end{array} \right. \tag{14.35}$$

The first order transport matrix of a solenoid with length L writes

$$T_{\mathrm{sol}} = \begin{pmatrix} C^2 & \frac{2}{K}SC & SC & \frac{2}{K}S^2 & 0 & 0 \\ \frac{-K}{2}SC & C^2 & -\frac{K}{2}S^2 & SC & 0 & 0 \\ -SC & -\frac{2}{K}S^2 & C^2 & \frac{2}{K}SC & 0 & 0 \\ \frac{K}{2}S^2 & -SC & -\frac{K}{2}SC & C^2 & 0 & 0 \\ 0 & 0 & 0 & 0 & 1 & \dfrac{L}{\gamma^2} \\ 0 & 0 & 0 & 0 & 0 & 1 \end{pmatrix} \quad \text{with} \quad \left[\begin{array}{l} K = \frac{B_s}{B\rho} \\ C = \cos\frac{KL}{2} \\ S = \sin\frac{KL}{2} \end{array} \right. \tag{14.36}$$

A solenoid rotates the decoupled axis longitudinally by an angle $\alpha = KL/2 = B_s L/2B\rho$.

14.5 Data Treatment Keywords

14.5.1 Concentration Ellipse: FAISCEAU, FIT[2], MCOBJET, ...

It is often useful to associate the projection of a particle bunch in the horizontal, vertical or longitudinal phase space with an *rms* phase space concentration ellipse (CE). Various keywords in `zgoubi` resort to concentration ellipses:

- FAISCEAU for instance prints out, in zgoubi.res, CE parameters drawn from individual particle coordinates

- random particle distributions by MCOBJET are defined using CE parameters.

- ellipse parameters computed from CEs are possible constraints in FIT[2] procedures.

Transverse phase space graphs by `zpop` also compute CEs.

The CE method is resorted to in various exercises, for instance for comparison of the ellipse parameters it gets from the *rms* matching of a bunch, with theoretical beam parameters, as derived from first order transport formalism or computed from rays by MATRIX, or TWISS.

The method used in these various keywords and data treatment procedures is the following. Let $z_i(s)$, $z_i'(s)$ be the phase space coordinates of $i = 1, n$ particles in a set observed at some azimuth s along a beam line or in a ring. The second moments of the particle distribution are

$$
\begin{aligned}
\overline{z^2}(s) &= \frac{1}{n}\sum_{i=1}^{n}(z_i(s)-\overline{z}(s))^2 \\
\overline{zz'}(s) &= \frac{1}{n}\sum_{i=1}^{n}(z_i(s)-\overline{z}(s))(z'_i(s)-\overline{z'}(s)) \\
\overline{z'^2}(s) &= \frac{1}{n}\sum_{i=1}^{n}(z'_i(s)-\overline{z'}(s))^2
\end{aligned}
\tag{14.37}
$$

From these, a concentration ellipse (CE) is drawn, encompassing a surface $S_z(s)$, with equation

$$\gamma_c(s)z^2 + 2\alpha_c(s)zz' + \beta_c(s)z'^2 = S_z(s)/\pi \tag{14.38}$$

Noting $\Delta = \overline{z^2}(s)\,\overline{z'^2}(s) - \overline{zz'}^2(s)$, the ellipse parameters write

$$\gamma_c(s) = \frac{\overline{z'^2}(s)}{\sqrt{\Delta}},\ \ \alpha_c(s) = -\frac{\overline{zz'}(s)}{\sqrt{\Delta}},\ \ \beta_c(s) = \frac{\overline{z^2}(s)}{\sqrt{\Delta}},\ \ S_z(s) = 4\pi\sqrt{\Delta} \tag{14.39}$$

With these conventions, the *rms* values of the z and z' projected densities satisfy

$$\sigma_z = \sqrt{\beta_z\frac{S_z}{\pi}} \quad \text{and} \quad \sigma_{z'} = \sqrt{\gamma_z\frac{S_z}{\pi}} \tag{14.40}$$

14.5.2 Transport Coefficients: MATRIX, OPTICS, TWISS, etc.

`Zgoubi` does not know about matrix transport, it does not define optical elements by a transport matrix, it defines them by electrostatic and/or magnetic fields in space (and time possibly). Well, except for a couple of optical elements, for instance TRANSMAT, which pushes particle coordinates using a matrix, or SEPARA, an analytical mapping through a Wien filter. `Zgoubi` does not transport particles using matrix products either, it does that by numerical integration of Lorentz force equation.

However it is often useful to dispose of a matrix representation of an optical element, of the transport matrix of a beam line, or the first or second order one-turn matrix of a ring accelerator. It may also be useful to compute the beam matrix and its transport. Several commands in `zgoubi` perform the necessary particle coordinates treatment to derive these informations. Examples are MATRIX: computation of matrix transport coefficients up to 3rd order, from initial and current coordinates of a particle sample. OPTICS transports a beam matrix, given its initial value using OBJET[KOBJ=5.1] (see Sect. 14.5.2.2). TWISS derives a periodic beam matrix from a 1-turn mapping of a periodic sequence, and transports it from end to end so generating the optical functions along the sequence (Sects. 14.5.2.2, 14.5.2.3).

These capabilities are used the exercises. It may be required for instance to compare transport coefficients derived from raytracing, with the matrix model of the optical element(s) concerned. Or to compute a periodic beam matrix in a periodic optical sequence, this is how betatron functions are produced, often for the mere purpose of comparisons with matrix code outcomes, or with expectations from analytical models.

14.5.2.1 Coordinate Transport

In the Gauss approximation (*i.e.*, with θ the angle of a trajectory to the reference axis, $\sin\theta \sim \theta$), particles follow paths which can be described with simple functions: parabolic, sinusoidal or hyperbolic. A consequence is that a string of optical elements, and coordinate transport through the latter, can be handled with a simple mathematics toolbox. Taylor expansion (also known as transport) techniques are part of it, whereby a coordinate excursion v_{2i} (with index $i = 1 \rightarrow 6$ standing for $x,\ x',\ y,\ y',\ \delta s$ or $\delta p/p$) from some reference trajectory at a location s_2 along the line is obtained from the excursions v_{1i} at an upstream location s_1, via

$$v_{2i} = \sum_{j=1}^{6} R_{ij}\, v_{1j} + \sum_{j,k=1}^{6} T_{ijk}\, v_{1j}\, v_{1k} + \sum_{j,k,l=1}^{6} v_{1ijkl}\, v_{1j}\, v_{1k}\, v_{1l} + \ \ldots \qquad (14.41)$$

This Taylor development can be written under matrix form, for instance to the first order in the coordinates, for non-coupled motion,

$$\begin{pmatrix} x \\ x' \\ y \\ y' \\ \delta s \\ \delta p/p \end{pmatrix}_2 = \begin{pmatrix} T_{11} & T_{12} & 0 & 0 & 0 & T_{16} \\ T_{21} & T_{22} & 0 & 0 & 0 & T_{26} \\ 0 & 0 & T_{33} & T_{34} & 0 & T_{36} \\ 0 & 0 & T_{43} & T_{44} & 0 & T_{46} \\ 0 & 0 & 0 & 0 & T_{55} & T_{56} \\ 0 & 0 & 0 & 0 & T_{65} & T_{66} \end{pmatrix} \begin{pmatrix} x \\ x' \\ y \\ y' \\ \delta s \\ \delta p/p \end{pmatrix}_1 = T(s_2 \leftarrow s_1) \begin{pmatrix} x \\ x' \\ y \\ y' \\ \delta s \\ \delta p/p \end{pmatrix}_1 \qquad (14.42)$$

These are the objects keywords as MATRIX [1, *cf.* Sect. 6.5] and OPTICS [1, *cf.* Sect. 6.4] compute: the values of the transport coefficients, or transport matrices to first and high order, are drawn from particle coordinates. Transport matrices of common optical elements (drift, dipole, quadrupole, etc., magnetic or electrostatic), are resorted to in the exercises for comparison with their matrix representation.

14.5.2.2 Beam Matrix

OPTICS and TWISS keywords cause the transport of a beam matrix. The former requires an initial matrix: it is provided as part of the initial object definition, by OBJET. The latter derives a periodic beam matrix from initial and final coordinates resulting from raytracing throughout an optical sequence. Basic principles are recalled here, This is the way it works in `zgoubi`, and in addition they are resorted to in the exercises.

In the linear approximation, the transverse phase space ellipse associated with a particle distribution (for instance, the concentration ellipse, Sect. 14.5.1) is written (with z standing for indifferently x or y)

$$\gamma_z(s)z^2 + 2\alpha_z(s)zz' + \beta_z(s)z'^2 = \frac{\varepsilon_z}{\pi} \tag{14.43}$$

in which the ellipse parameters

$$\beta_z(s), \;\; \alpha_z(s) = -\frac{1}{2}\frac{d\beta_z}{ds}, \;\; \gamma_z(s) = \frac{1+\alpha^2}{\beta_z} \tag{14.44}$$

are functions of the azimuth s along the optical sequence. The surface ε_z of the ellipse is an invariant if the beam travels in magnetic fields, however field non-linearities, phase space dilution, etc. may distort the distribution and change the surface of its *rms* matching concentration ellipse. In the presence of acceleration or deceleration the invariant quantity is $\beta\gamma\varepsilon_z$ instead, with $\beta = v/c$ and γ the Lorentz relativistic factor.

The ellipse Eq. 14.43 can be written under the matrix form

$$\mathbf{1} = \tilde{T}\,\sigma_z^{-1}T \tag{14.45}$$

with σ_z the beam matrix:

$$\sigma_z = \frac{\varepsilon_z}{\pi}\begin{pmatrix} \beta_z & -\alpha_z \\ -\alpha_z & \gamma_z \end{pmatrix} \tag{14.46}$$

The ellipse parameters can be transported from s_1 to s_2 using

$$\sigma_{z,2} = T\,\sigma_{z,1}\,\tilde{T} \tag{14.47}$$

with $T = T(s_2 \leftarrow s_1)$ the transport matrix (Eq. 14.42) and $\tilde{T}$ its transposed. This can also be written under the form

$$\begin{pmatrix} \beta_z \\ \alpha_z \\ \gamma_z \end{pmatrix}_2 = \begin{pmatrix} T_{11}^2 & -2T_{11}T_{12} & T_{12}^2 \\ -T_{11}T_{21} & T_{21}T_{12}+T_{11}T_{22} & -T_{12}T_{22} \\ T_{21}^2 & -2T_{21}T_{22} & T_{22}^2 \end{pmatrix}_{s_2\leftarrow s_1} \begin{pmatrix} \beta_z \\ \alpha_z \\ \gamma_z \end{pmatrix}_1 \tag{14.48}$$

(subscripts 1, 2 normally hold for horizontal plane motion, $z = x$: change to 3, 4 for vertical motion, $z = y$). This beam matrix formalism can be extended to the longitudinal phase space and coordinates (δs, $\delta p/p$), a 6×6 beam matrix can be defined,

$$\sigma = \begin{pmatrix} \sigma_{11} & \sigma_{12} & 0 & 0 & 0 & \sigma_{16} \\ \sigma_{21} & \sigma_{22} & 0 & 0 & 0 & \sigma_{26} \\ 0 & 0 & \sigma_{33} & \sigma_{34} & 0 & \sigma_{36} \\ 0 & 0 & \sigma_{43} & \sigma_{44} & 0 & \sigma_{46} \\ 0 & 0 & 0 & 0 & \sigma_{55} & \sigma_{56} \\ 0 & 0 & 0 & 0 & \sigma_{65} & \sigma_{66} \end{pmatrix} \tag{14.49}$$

This can be generalized to non-zero anti-diagonal coupling terms, if motions are coupled.

14.5.2.3 Periodic Structures

In the hypothesis of an S- periodic structure: a long beam line with repeating pattern, a cyclic accelerator, transverse motion stability requires the transport matrix over a period, from s to $s + S$ to satisfy

$$[T_{ij}](s + S \leftarrow s) = I \cos\mu + J \sin\mu \tag{14.50}$$

where $\mu = \int_{(S)} ds/\beta$ is the betatron phase advance over the period (independent of the origin),

$$I = \begin{pmatrix} 1 & 0 \\ 0 & 1 \end{pmatrix} \text{ is the identity matrix, } J = \begin{pmatrix} \alpha_z(s) & \beta_z(s) \\ -\gamma_z(s) & -\alpha_z(s) \end{pmatrix} \text{ (and } J^2 = -I) \tag{14.51}$$

14.6 Exercises

14.1 Magnetic Sector Dipole

Solution: page 599.

(a) Simulate a $\rho = 1$ m radius, $\alpha = 60$ degree sector dipole with n=-0.6 field index, in both cases of hard edge and of soft fall-off fringe field model. Find the reference arc, such that $\int_{\text{arc}} B\, ds = BL$ with L the arc length in the hard-edge model and B the field along that arc.

Make sure that the reference arc has the expected length.

Produce the field along the reference arc, for a few different values of the fringe-field extent.

(b) A possible check of the first order: OBJET[KOBJ=5], MATRIX[IORD=1,IFOC=0] can be used to compute the transport matrix from the rays. Compare what it gives with theory.

Fig. 14.12 Symmetric point to point focusing

(c) Consider a sector dipole with parallel gap, uniform field. Show the well known geometrical property of point-to-point focusing represented in Fig. 14.12.

Test the convergence of the numerical solution versus integration step size.

(d) Transport a proton along the reference axis, injected with its spin tangent to the axis. Compare spin rotation with theory.

Test the convergence of the numerical solution versus integration step size.

14.2 Quadrupole Doublet

Solution: page 604.

Reproduce Fig. 14.9.

14.3 Solenoid

Solution: page 605.

An introduction to SOLENOID.

(a) Reproduce Fig. 14.11. Use both fields models of Eqs. 14.31, 14.34 and compare their outcomes, including the first order paraxial transport matrices, higher order as well (computed from in and out trajectory coordinates).

(b) Compare final coordinates in (a) with outcomes from the first order transport formalism (Sect. 14.4.3).

(c) Make a 1-dimensional (on-axis) field map of a $r_0 = 10$ cm, $L = 1$ m solenoid (namely, a map $B_{\mathrm{X,i}}(X_i)$ of the field at the nodes of a X-mesh with mesh size $X_{\mathrm{i+1}} - X_i$). Reproduce the trajectory in (a) (case $r_0 = 10$ cm) using that field map, with the keyword BREVOL. Check the convergence of the final particle coordinates, using the field map, depending on the mesh size.

14.7 Solutions of Exercises of Chapter 3: Optical Elements and Keywords, Complements

14.1 Magnetic Sector Dipole

DIPOLE input data.

(a) A simulation of a $\rho = 0.5$ m radius, 60 degree sector dipole with n=-0.6 field index, in the hard-edge field model, is given in Tab. 14.1. A simulation which includes fringe fields is given in Tab. 14.2.

A major difference between the two is in the angular extent of the field domain, AT, in order to allow encompassing the fringe field extents, however there is more, as follows.

Hard edge model

The effective field boundaries (EFB) have to be placed on the angular opening limits, which means, in the representation of Fig. 14.13, and according to the users' guide [13, see DIPOLE],

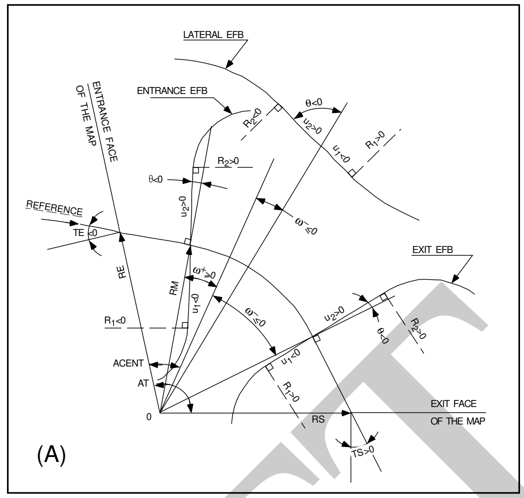

Fig. 14.13 Parameters used to define the geometry of a dipole magnet with index, using DIPOLE [13, see DIPOLE]

$$\omega^+ = ACENT > 0, \quad \omega^- = -ACENT < 0, \quad \omega^+ - \omega^- = AT > 0$$

Otherwise, in the case AT would be greater than the magnet deflection angle α = 60 deg, particles would jump from zero field to plateau field value over the EFB, and so miss part of the field integral. Note that for mere code-specific, geometry computation reasons, it also requires that ACENT=AT/2, so that, *in fine*, $\omega^+ = -\omega^- = ACENT/2$.

Soft edge model

AT has to be greater than the magnet deflection angle $\alpha = 60$ deg in order to encompass the fringe field extent beyond the entrance and exit EFBs, so that, in the representation of Fig. 14.13, and according to the users' guide,

$$ACENT > \omega^+, \qquad |\omega^-| < AT - ACENT$$

Integration-wise, particles will smoothly traverse the field fall-off regions, step by step, no field discontinuity there. Note that motion integration accuracy requires the step size to be small enough, compared to the fringe field extent. In the notations of Fig. 14.13, the resulting additional optical axis lengths l_E and l_S within the AT sector, on entrance and exit side respectively, to account for the field fall-offs, write

$$l_E = RM \times \tan(ACENT - \omega^+), \qquad l_S = RM \times \tan[AT - (ACENT - \omega^-)]$$

Checking back one fortunately finds

$$\underbrace{\operatorname{atan}\left(\frac{l_E}{RM}\right)}_{\substack{\text{entrance}\\ \text{fringe field}}} + \underbrace{\omega^+ - \omega^-}_{\text{magnet body}} + \underbrace{\operatorname{atan}\left(\frac{l_S}{RM}\right)}_{\substack{\text{exit}\\ \text{fringe field}}} = AT$$

It also results from the fringe field modeling that the reference trajectory (which is ideally the trajectory that coincides with R=RM in the body of the magnet) enters the AT sector at radius RE, with an incidence TE. These two quantities have to be accounted for in setting the entrance and exit reference frames, however this is user's matter, regarding the choice of reference frames: most often (in synchrotron rings for instance) the reference curve is R=RM, so that Y and T coordinates of the reference particle are zero (the moving frame has its origin at the origin of the polar frame in which the field is defined, and rotates with the particle, clockwise in Fig. 14.13 representation). Thus, one has to set

$$TE = -(ACENT - \omega^+) < 0, \qquad RE = RM/\cos TE$$

Note that, because of the small deflection due to fringe fields, RS and TS need be adjusted if the DIPOLE process has to end up with the reference particle featuring zero Y and T coordinates. Expectedly, that would be satisfied with RS and TS values near

$$TS = AT - (ACENT - \omega^-) > 0, \qquad RS = RM/\cos TS$$

The radius R of the reference arc, such that $\int_{\mathrm{arc}} B\,ds = BL$ with L the arc length in the hard-edge model, has to be found. Same thing for the arcs at ±0.1% momentum offset. FIT can be used for that.

(b) First order transport.

This is left to the reader. Theoretical matrices are given in Eqs. 14.7, 14.8.

Refer to exercises in earlier chapters, such comparison is often performed.

(c) Point-o-point focusing.

The DIPOLE of Tab. 14.1 can be used, with the following change and addenda:
- set the field index to zero in DIPOLE
- add OBJET[KOBJ=1,IMAX=41] so to generate 41 particles launched with $T_0 \in [-20, 20]$ mrad, like so:

```
'OBJET'
64.62444403717985
1
1   41  1  1  1  1
0.  1.  0. 0. 0. 0.
50. 0.  0. 0. 0. 3.8685052339
```

- add AUTOREF[I=2] after DIPOLE: that will cause the moving frame to move to the waist formed by particles 1, 3 and 5.

- add FAISTORE[FNAME=zgoubi.fai,IP=1] after AUTOREF, before END. This logs particle data at that location.

Table 14.1 Input data file: definition of a dipole with index in the hard-edge field model. Definition of the [#S_60dSectDip_hardE:#E_60dSectDip_hardE] segment, mostly for the purpose of possible further INCLUDE. This file is used under the name sectorDIP_hardE.inc in subsequent exercises

```
! File sectorDIP.inc (hard-edege, here)
'MARKER'   #S_60dSectDip_hardE                          ! Label should not exceed 20 characters.
'DIPOLE'                                               ! Analytical definition of a dipole field.
2                 ! IL=2, only purpose is to logged trajectories to zgoubi.plt, for further plotting.
60. 50.                                                   ! Sector angle AT; reference radius RM.
30. 5. -0.6 0. 0.         ! Reference azimuthal angle ACN; BM field at RM; indices, N=-0.6 at RM=50cm.
0.  0.                                                                      ! EFB 1 is  hard-edge,
4  .1455   2.2670  -.6395  1.1558  0. 0.  0.             ! hard-edge only possible with sector magnet.
30. 0.  1.E6  -1.E6  1.E6  1.E6
0.   0.                                                                                   ! EFB 2.
4  .1455   2.2670  -.6395  1.1558  0. 0.  0.
-30. 0.  1.E6  -1.E6  1.E6  1.E6
0. 0.                                                                            ! EFB 3 (unused).
0  0.      0.      0.      0.      0. 0.  0.
0. 0.  1.E6  -1.E6  1.E6  1.E6 0.
4   10.
0.5                        ! Integration step size. The smaller, the more accurately the orbits close.
2  0. 0. 0. 0.                                                ! Magnet positionning RE, TE, RS, TS.
'MARKER'   #E_60dSectDip_hardE                          ! Label should not exceed 20 characters.
'END'
```

Table 14.2 Input data file: definition of a dipole with index in the soft-edge field model. The field extent in the Enge model (Eq. 14.5) is taken to be $g = 5\,\mathrm{cm}$ ($\lambda_E = \lambda_S = g$ in the guide's notations), so subtended by an angle $\mathrm{atan}(g/RM) = 5.71059\,\mathrm{deg}$, thus well comprised in a 10 deg angular aperture. ACENT value is free, 30 deg as adopted here is arbitrary, it is just left to the value it was given in the hard edge settings (Tab. 14.1). This input includes the definition of the [#S_60dSectDip_softE:#E_60dSectDip_softE] segment. This file is used under the name sectorDIP_softE.inc in subsequent exercises

```
! File sectorDIP.inc (soft-edege, here)
'MARKER'    #S_60dSectDip_softE                          ! Label should not exceed 20 characters.
'DIPOLE'                                               ! Analytical definition of a dipole field.
2                 ! IL=2, only purpose is to logged trajectories to zgoubi.plt, for further plotting.
80. 50.                 ! Sector angle AT=60 deg deflection+2*10deg for fringes; reference radius RM.
30. 5. -0.6 0. 0.  ! Reference angle ACENT (arbitrary value); field at RM; indices, N=-0.6 at RM=50cm.
5. 0.    ! Entry EFB: lambda~gap=5 cm, well comprised in RM*tan(10deg)=; same gap at all R -> nappa=0.
4  .1455  2.2670  -.6395  1.1558  0. 0.  0.                            ! Enge coefficients at entry.
20. 0. 1.E6 -1.E6 1.E6 1.E6 ! omega^+ = +20 deg from ACENT leaves 10deg room (8.8cm) for entry fringe.
5. 0.     ! Exit EFB: lambda~gap=5 cm, well comprised in RM*tan(10deg)=; same gap at all R -> nappa=0.
4  .1455  2.2670  -.6395  1.1558  0. 0.  0.                             ! Enge coefficients at exit.
-40. 0. 1.E6 -1.E6 1.E6 1.E6  ! omega^- =-40 deg from ACENT leaves 10deg room (8.8cm) for exit fringe.
0. 0.                                                                            ! EFB 3 (unused).
0  0.      0.      0.      0.      0. 0.  0.
0. 0.  1.E6  -1.E6  1.E6  1.E6 0.
4   10.
0.5                        ! Integration step size. The smaller, the more accurately the orbits close.
2  0. 0. 0. 0.                                                ! Magnet positionning RE, TE, RS, TS.
'MARKER'    #E_60dSectDip_softE                          ! Label should not exceed 20 characters.
'REBELOTE'

'END'
```


The following gnuplot script will print the horizontal phase space (Fig. 14.14)

```
cm2m = 1e-2; mrd2rd = 1e-3
plot './zgoubi.fai' u ($10 *cm2m):($11 *mrd2rd) w p ps .9 pt ; pause 2
```

In the execution listing zgoubi.res one finds:

```
  3  Keyword, label(s) :  AUTOREF
 Change  of  reference,  horizontal,   XC = -0.0 cm , YC = 49.99999996 cm ,   A =  -0.000000 deg
 TRAJ 1 IEX,D,Y,T,Z,P,S,time :  1   3.869  3.2398E-22  0.  0.  0.  157.08  5.23961E-03
```

This indicates that AUTOREF found the waist
- at $XC = 0$, which means at the exit EFB of the dipole,
- at a radial excursion $YC = 50\,\mathrm{cm}$ as expected (the origin of the Y axis is at DIPOLE curvature center),

Table 14.3 Input data file: find closed orbits, using FIT or FIT2, and log stepwise data in zgoubi.plt. Closed orbits are found for the reference particle (a particle with rigidity $B\rho = 5_{[\mathrm{kG}]} \times 50_{[\mathrm{cm}]}$ kG cm) and for particles with $\pm\delta p/p$ momentum offset. FIT starts with initial Y_0 radius values resulting from a hard edge model, *i.e.*, $Y_0 = B\rho/B = 250_{[kG\,cm]}/5_{[kG]}$ and ± 0.1%. This file produces the field along these trajectories, an effect of DIPOLE[IL=2]. The [#S_60dSectDip_softE:#E_60dSectDip_softE] segment of Tab. 14.2 is INCLUDEd; simply substitute [#S_60dSectDip_hardE:#E_60dSectDip_hardE] (as defined in Tab. 14.1) to work with the hard edge model instead

```
Uniform field sector with index. Field on orbits at different momenta.
'MARKER'   DIPOLEField_S                                                  ! Just for edition purposes.
!                                              First stage: find closed orbit at 1 MeV, for some k value.
'OBJET'
64.62444403717985                        ! Reference Brho ("BORO" in the users' guide) -> 200keV proton.
2                                                                       ! Particles are defined one by one.
3 1                                                      ! 3 particles, classified in a single momentm set.
50. 0. 0. 0. 0. 3.8685052339 'o'                          ! Y_0=50cm is hard edge case -> 2.9886MeV proton.
50.125472 0. 0. 0. 0. 3.8723737392 'p'      ! +0.001 mom. offset. Circular orbit Y_0 is hard edge case.
49.875465 0. 0. 0. 0. 3.8646367287 'm'      ! -0.001 mom. offset. Circular orbit Y_0 is hard edge case.
1 1 1                  ! As many '1' as there are particles (that dates from programs on punched cards!
'INCLUDE'
1
./sectorDIP.inc[#S_60dSectDip_softE:#E_60dSectDip_softE]          ! DIPOLE with fringe, RM=50cm n=-0.6.
!./sectorDIP.inc[#S_60dSectDip_hardE:#E_60dSectDip_hardE]      ! DIPOLE with hard-edge, RM=50cm n=-0.6.
 'FIT'                                              ! This matching procedure finds the closed orbit radius.
3   nofinal
2  30  0  .9                                                  ! Variable : Y_0. Variation allowed up to 90%.
2  40  0  .9                                                  ! Variable : Y_0. Variation allowed up to 90%.
2  50  0  .9                                                  ! Variable : Y_0. Variation allowed up to 90%.
3  1e-15  99                                                   ! Penalty; max numb of calls to the function.
3.1 1 2 #End 0. 1. 0                                                ! Constraint :  Y_final=Y_0, particle 1.
3.1 2 2 #End 0. 1. 0                                                ! Constraint :  Y_final=Y_0, particle 2.
3.1 3 2 #End 0. 1. 0                                                ! Constraint :  Y_final=Y_0, particle 3.
'MARKER'   DIPOLEField_E                                                  ! Just for edition purposes.
'END'
```

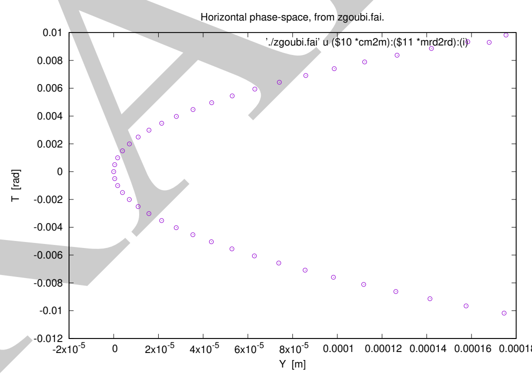

Fig. 14.14 Aberration curve at the focal point of a 180 deg uniform field dipole: a second order (sextupole) aberration, $Y \propto T^2$, typical of a bend non-linearities

- with the reference frame X axis at an angle $A = 0$ to particle 1 direction of motion.
QED.

In the case of an $\alpha = 60$ deg dipole, the previous input data file can be used, changing DIPOLE angles to $AT = \omega^+ - \omega^- = 60$ deg with for instance $\omega^+ = -\omega^- = 30$ deg. Drifts of identical lengths, DRIFT[$XL = RM/\tan(\alpha/2)$], have to be added upstream and downstream of DIPOLE in order to obtain the symmetrical configuration of Fig. 14.12.

Step size:

The method is the same as in exercise 2.2 (b), case of a toroidal condenser, which can be referred to.

(d) Spin precession.

Add SPNTRK[KSO=1] at the begining of the input data file to traack spin, starting aligned on the X axis. Tracking spin also requires PARTICUL, in order to define particle's mass, charge and anomalous magnetic moment.

The theoretical value of the spin precession angle in the moving frame is $G\gamma\alpha$ (Eq. 3.32), with $\alpha = \pi$ or $\alpha = \pi/3$ in the previous two deflection cases considered.

This is the value which the stepwise integration produces.

14.2 Quadrupole Doublet

The input dta file for this problem is given in Tab. 14.4.

Table 14.4 Input data file: a double-focus quadrupole doublet

```
100 particles on an ellipse, through drift
'OBJET'
1000.
2
9  1
0.  0. 0.  0. 0. 1. 'o'
0.  1. 0.  0. 0. 1. 'a'
0. -1. 0.  0. 0. 1. 'b'
0.  2. 0.  0. 0. 1. 'c'
0. -2. 0.  0. 0. 1. 'd'
0.  0. 0.  1. 0. 1. 'e'
0.  0. 0. -1. 0. 1. 'f'
0.  0. 0.  2. 0. 1. 'g'
0.  0. 0. -2. 0. 1. 'h'
1 1 1 1 1 1 1 1 1 1
'FAISCEAU'

'MARKER'  dum .plt
'DRIFT'
70.  split 100 2
'QUADRUPO'       QF
2
40. 10.  4.7907188    ! 11.1111
0. 0.
6  .1122 6.2671 -1.4982 3.5882 -2.1209 1.723
0. 0.
6  .1122 6.2671 -1.4982 3.5882 -2.1209 1.723
1.
1 0 0 0
'DRIFT'
100.  split 100 2
'QUADRUPO'       QD
2
40. 10. -4.7907188    ! -11.1111
0. 0.
6  .1122 6.2671 -1.4982 3.5882 -2.1209 1.723
0. 0.
6  .1122 6.2671 -1.4982 3.5882 -2.1209 1.723
1.
1 0 0 0
'DRIFT'
70.  split 100 2
'MARKER'  dum .plt
'FAISCEAU'

! 'FIT'                                                                    ! This FIT procedure
! 2                                                               ! varies QF and QD fields so to get
! 5 12 0 .4                ! common focus point in both planes, 3.2 meters downstream of the object.
! 7 12 0 .4
! 4  1E-15
! 3  6 2 #End 0. 1. 0
! 3 11 2 #End 0. 1. 0
! 3  2 4 #End 0. 1. 0
! 3  3 4 #End 0. 1. 0

'IMAGE'
'IMAGEZ'

'DRIFT'
20.  split 100 2

'END'
```

14.3 Solenoid

(a) The paraxial trajectory pitch is $l = 2\pi\, B\rho/B_0$ (Sect. 14.4.3). Take $L = 1\,\mathrm{m}$ (Fig. 14.11) and $B\rho = 1\,\mathrm{T\,m}$ for simplicity, thus $B_0 = 2\pi\,\mathrm{T}$. Assume a particle launched from $Y = Z = 1\,\mathrm{mm}$ with zero incidence. Scan the solenoid radius value in the range $1 \le r_0 \le 200\,\mathrm{mm}$ to reproduce the figure. The data to be plotted $(X,\ Y,\ Z,\ B_X)$ are read from zgoubi.plt.

The beam optics model is given in Tab. 14.5. Note the use of KOBJ=2 in OBJET, which allows creating particles in an arbitrary number (just one, here), with arbitrary initial coordinates. REBELOTE[IOPT=1] is used to repeat the sequence, varying the parameter R_0 under SOLENOID.

Table 14.5 Input data file: a 1 m long solenoid, with 1 m upstream and downstream fringe field extents. The initial coil radius is $r_0 = 0.1$ cm, it is scanned (by REBELOTE) over the range $1 \le r_0 \le 20$ cm. For each r_0 a particle is launched with initial position $Y = Z = 1$ mm and initial angles $T = P = 0$

```
A 1 meter long solenoid.
'MARKER'  opticalLmntsProbSolenoA_S
'OBJET'
1000.
2                                                              ! OBJET style KOBJ=2.
1 1
0.1  0. 0.1 0. 0. 1. 'o'                ! Initial coordinates Yo, To, Zo, Po, Xo, Do.
1
'SOLENOID'
200                        ! Log particle data to zgoubi.plt, every other 100 steps.
100.  .1  62.8318530718     ! length (cm); radius (cm); field (kG); [MODL=1] default.
100. 100.            ! Extent of integration regions upstream and downstream of coil.
.01
1  0. 0. 0.
'FAISCEAU'
'REBELOTE'                                             ! Used to repeat the sequence.
10 0.1 0  1                                                        ! Repeat 10 times.
1
SOLENOID 11 1.:20.                         ! Vary parameter 11 (= R0) under SOLENOID.
'MARKER'  opticalLmntsProbSolenoA_E
'END'
```

Table 14.6 Input data file: track a particle along the central axis of the solenoid, to generate a 3 m long, 1D field map, with mesh step 5 cm

```
! A 3 meter long solenoid field map.
'MARKER'  opticalLmntsProbSolenoC_S
'OBJET'
1000.
2                                                              ! OBJET style KOBJ=2.
1 1
0.  0. 0. 0. 0. 1. 'o'                  ! Initial coordinates Yo, To, Zo, Po, Xo, Do.
1
'SOLENOID'
200                        ! Log particle data to zgoubi.plt, every other 100 steps.
100.  .1  62.8318530718     ! length (cm); radius (cm); field (kG); [MODL=1] default.
100. 100.            ! Extent of integration regions upstream and downstream of coil.
5.
1  0. 0. 0.
'FAISCEAU'
'END'
```

(b) To allow comparison, theoretical matrices (Eq. 14.36) must be computed for the theoretical length, L, of the matrix transport solenoid model. Tracking must extend upstream and downstream of the solenoid, over a distance much greater than the solenoid diameter (the latter determines the field fall extent, Eq. 14.31).

(c) A 1-dimensional (on-axis) field map of the solenoid field, $B_{X,i}(X_i)$, can simply be generated by tracking a particle along the solenoid axis. It has to extend upstream and downstream of the solenoid, over a distance much greater than the solenoid diameter. The integration step size will be the mesh size, take it in the centimeter range ($\lesssim r_0$), 5 cm here. An intermediate stage is necessary, which consists in reading $X, B_X(X)$ from zgoubi.plt and re-writing it in a dedicated ASCII file in a format proper for use by the keyword BREVOL.

The input file to generate the field and log to zgoubi.plt is given in Tab. 14.6.

Similar exercises, generating a 1D field map and using BREVOL, can be found be found in `zgoubi` sourceforge repository [14].

Table 14.7 Input data file: track a particle in the solenoid, in a similar manner to the input data file of Tab. 14.6, using a field map model instead

```
A 1 meter long solenoid, 3 meter long field map.
'OBJET'
1000.
2
1 1
0.  0. 0. 0. 0. 1. 'o'
1
'BREVOL'
0 0
1. 1.
Test solenoid 1D field map
61                                          ! Number of nodes of the 1D mesh.
solenoid_1meter.map
0  0. 0. 0.
2
1.
1 0 0 0
'FAISCEAU'
'END'
```

References

1. Méot, F.: Zgoubi Users' Guide. https://www.osti.gov/biblio/1062013-zgoubi-users-guide Sourceforge latest version: https://sourceforge.net/p/zgoubi/code/HEAD/tree/trunk/guide/Zgoubi.pdf
2. The AGS at the Brookhaven National Laboratory: https://www.bnl.gov/rhic/AGS.asp
3. The CERN PS: https://home.cern/science/accelerators/proton-synchrotron
4. Volk, James T.: Experiences with permanent magnets at the Fermilab recycler ring. James T Volk 2011 JINST6 T08003. https://iopscience.iop.org/article/10.1088/1748-0221/6/08/T08003/pdf
5. Dutheil, Y.: A model of the AGS based on stepwise ray-tracing through the measured field maps of the main magnets. Proceedings of IPAC2012, New Orleans, Louisiana, USA, TUPPC101, 1395-1399.
   https://accelconf.web.cern.ch/IPAC2012/papers/tuppc101.pdf
   Méot, et al.: Modeling of the AGS using `zgoubi` - status. Proceedings of IPAC2012, New Orleans, Louisiana, USA, MOPPC024, 181-183.
   https://accelconf.web.cern.ch/IPAC2012/papers/moppc024.pdf
6. Enge, H. A.: Deflecting magnets. In: Focusing of Charged Particles, ed. A. Septier, Vol. II, pp. 203-264, Academic Press Inc., 1967
7. Thern, R. E, Bleser, E.: The dipole fields of the AGS main magnets, BNL-104840-2014-TECH, 1/26/1996.
   https://technotes.bnl.gov/PDF?publicationId=31175
8. Méot, F., Ahrens L., Brown, K., et al.: A model of polarized-beam AGS in the ray-tracing code Zgoubi. BNL-112453-2016-TECH, C-A/AP/566 (July 2016). https://technotes.bnl.gov/PDF?publicationId=40470
   https://www.osti.gov/biblio/1336073
9. Méot, F., Lemuet, F.: Developments in the ray-tracing code Zgoubi for 6-D multiturn tracking in FFAG rings. NIM A 547 (2005) 638-651.
10. Leleux, G.: Accélérateurs Circulaires. Lectures at the Institut National des Sciences et Techniques du Nucléaire, CEA Saclay (July 1978), unpublished
11. Credit: Brookhaven National Laboratory.
    https://www.flickr.com/photos/brookhavenlab/8495311598/in/album-72157611796003039/
12. Garrett, M.W.: Calculation of fields [...] by elliptic integrals. In: J. Appl. Phys., 34, 9, Sept. 1963
13. Méot, F.: Zgoubi Users' Guide.
    https://www.osti.gov/biblio/1062013-zgoubi-users-guide Sourceforge revision 1379 (2020-

02-29): https://sourceforge.net/p/zgoubi/code/HEAD/tree/trunk/guide/Zgoubi.pdf

14. https://sourceforge.net/p/zgoubi/code/HEAD/tree/branches/exemples/KEYWORDS/BREVOL/